JOURNAL OF GEOPHYSICAL RESEARCH, VOL. 107, NO. B7, 10.1029/2001JB000521, 2002

Paleomagnetism of the early Triassic Semeitau igneous series, eastern Kazakstan

John J. Lyons, Robert S. Coe, and Xixi Zhao
Department of Earth Sciences, University of California, Santa Cruz, California, USA

Paul R. Renne
Berkeley Geochronology Center, Berkeley, California, USA

Alexey Y. Kazansky, Andrey E. Izokh, Leonid V. Kungurtsev, and Dimitry V. Mitrokhin
United Institute of Geology, Geophysics, and Mineralogy, Novosibirsk, Russia

Received 21 March 2001; revised 2 November 2001; accepted 7 November 2001; published 23 July 2002.

[1] Paleomagnetic results obtained from the early Triassic Semeitau igneous series (SIS) yield a high-quality pole for eastern Kazakstan that is concordant with reference poles for Siberia and Europe, strongly supporting the hypothesis that Kazakstan was already joined with Eurasia at this time. Of the 25 sites that were measured, data were straightforward for 20 sites, 2 of which recorded normal polarity and 18 of which recorded reverse; 5 sites were discarded because of severe overprinting, unstable demagnetizations, or extremely scattered within-site directions. Combining sites judged to be the same cooling unit and taking the average of 15 cooling units of equal weight, we calculated a pole located at 56°N, 139°E ($N = 15$, $K = 24.6$, $\alpha_{95} = 7.9$) for the SIS. We consider this pole to be reliable. The sampling of temporally spaced extrusives and more slowly cooled intrusives and the presence of both polarities strongly suggest that this pole averages secular variation. The $^{40}Ar/^{39}Ar$ determinations on sanidine crystals from two extrusive units yielded highly consistent ages of 248.2 ± 0.5 and 248.8 ± 0.5 Ma. Comparison of our pole for the SIS with the Siberian reference pole shows relative translation (−8° ± 10°) and rotation (1° ± 16°) that are indistinguishable from zero at 95% confidence. This result fails to confirm hypothesized post-Permian rotation of the Siberian craton relative to its margins and provides no evidence for left-lateral motion on the east-west shear zones in which the Semeitau is located. The similarity of ages between the SIS and the Siberian Traps supports speculation of a genetic relationship between the two. *INDEX TERMS:* 1525 Geomagnetism and Paleomagnetism: Paleomagnetism applied to tectonics (regional, global); 8110 Tectonophysics: Continental tectonics—general (0905); 8157 Tectonophysics: Plate motions—past (3040); 9320 Information Related to Geographic Region: Asia; *KEYWORDS:* Triassic paleomagnetism, Kazakstan, Semeitau igneous series, $^{40}Ar/^{39}Ar$ dates, Siberia Traps, Asian tectonics

1. Introduction

[2] The tectonic history of central Asia is complicated; numerous questions remain regarding the coherence of the Siberian craton and the amalgamation of the central Asian tectonic blocks. Paleomagnetism is an important tool for unraveling such tectonic problems, but its effective use requires high-quality data from all regions under consideration. On the basis of the concordance of paleomagnetic data, *Khramov* [1982], *Zhao et al.* [1990], *Bazhenov et al.* [1999], and others argue that Kazakstan has been part of Eurasia since the mid-Permian. These arguments, however, derive from paleomagnetic directions that are either not well documented in the literature [*Khramov*, 1982; *Zhao et al.*, 1990] or from inclination-only data in the Tien Shan region [*Bazhenov et al.*, 1999]. Other data that exist for the Kazakstan plate for this time period are poorly documented [*Didenko et al.*, 1994], incompletely demagnetized [*Sholpo and Rusinov*, 1971; *Kumpan et al.*, 1986; *Rusinov*, 1986], or suffer from inclination shallowing [*Bazhenov et al.*, 1995]. A complete examination of the hypothesis of the tectonic coherence of Kazakstan and Eurasia requires well-documented studies from several areas of the Kazakstan plate. As a first step in this direction, we present paleomagnetic results from the early Triassic Semeitau igneous series (SIS) of eastern Kazakstan.

[3] The paleomagnetic data presented here also have bearing on hypotheses of substantial internal deformations of the Eurasian continent since amalgamation. *Bazhenov and Mossakovsky* [1986] cited evidence for Mesozoic clockwise rotation of the Siberian craton relative to the Russian craton and the Kazakstan plate. This hypothesis predicts that directions from Kazakstan would be rotated

0148-0227/02/2001JB000521$09.00

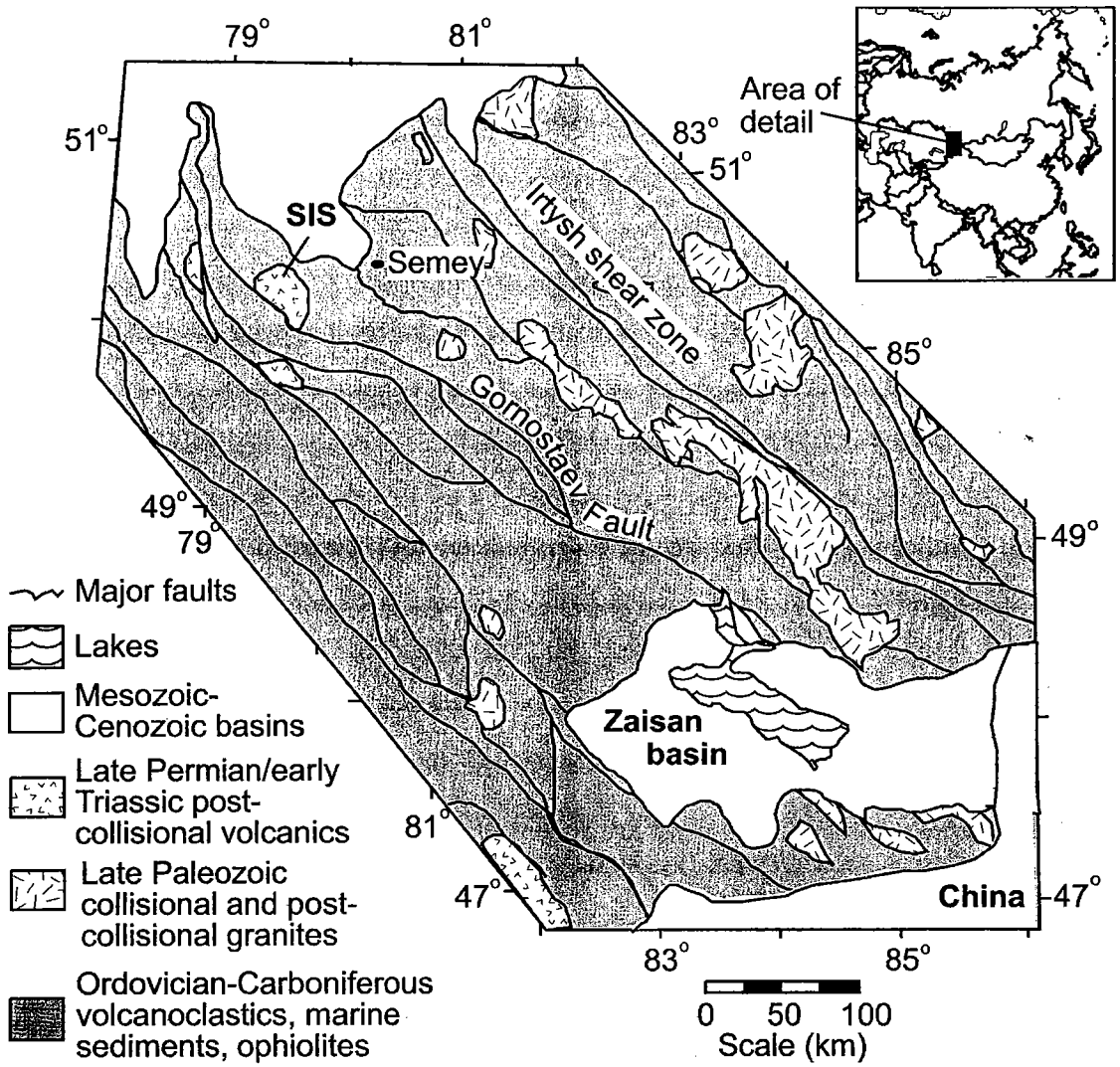

Figure 1. Map of eastern Kazakstan, showing the location of the SIS, late Paleozoic early Mesozoic igneous bodies, major faults, towns, and basins. Simplified from *Berzin et al.* [1994]. Inset shows the location of this map in the context of Asia.

counterclockwise relative to those of a similar age from the Siberian craton. *Allen et al.* [1995] and *Şengör and Natal'in* [1996] also cited evidence for late Permian to early Triassic clockwise motion of Siberia relative to the Russian craton, motion accommodated by left-lateral shear along the Gornostaev and Irtysh shear zones (Figure 1). Had such left-lateral motion occurred, we would expect paleomagnetic directions from blocks within the shear zone to be rotated counterclockwise relative to Europe.

[4] Around the Permo-Triassic boundary, central Asia and Siberia were sites of extensive magmatism that comprise the voluminous Siberian Traps and a broad swath of alkaline and bimodal bodies that extends from central and southern Kazakstan across southern Siberia, and possibly farther (Figure 2). The exact timing of the these magmatic events could have a significant bearing on the cause of the Permo-Triassic mass extinction and on the recent debate over the plume versus nonplume origin for the Siberian Traps [e.g., *Basu et al.*, 1995; *Czamanske et al.*, 1998].

[5] Although the age of the Siberian Traps is well constrained by $^{40}Ar/^{39}Ar$ and U-Pb dating [*Renne et al.*, 1995; *Basu et al.*, 1995; *Dalrymple et al.*, 1995; *Kamo et al.*, 1996; *Venkatesan et al.*, 1997], available dates for the alkaline and bimodal bodies are far less reliable and precise than K-Ar and Rb-Sr ages. As a result, there is little agreement on the spatiotemporal relationships among the igneous bodies [e.g., *Kurchavov and Yarmolyuk*, 1985; *Coleman*, 1989; *Kostitsyn*, 1996; *Dobretsov*, 1997]. The most notable analysis of the age data is that of *Dobretsov* [1997], who suggests that a large spreading plume event, similar to that proposed for the Cretaceous Pacific [*Larson*, 1991] or Cenozoic Africa [*Ebinger and Sleep*, 1998], was the cause of both the Siberian Traps and the alkaline/bimodal magmatism. There is, however, no general agreement that the Siberian Traps were initiated by a plume but rather much debate for [e.g., *Renne and Basu*, 1991; *Basu et al.*, 1995; *Dobretsov*, 1997, and references therein] and against [e.g., *Czamanske et al.*, 1998; *Elkins-Tanton and Hager*, 2000] the plume

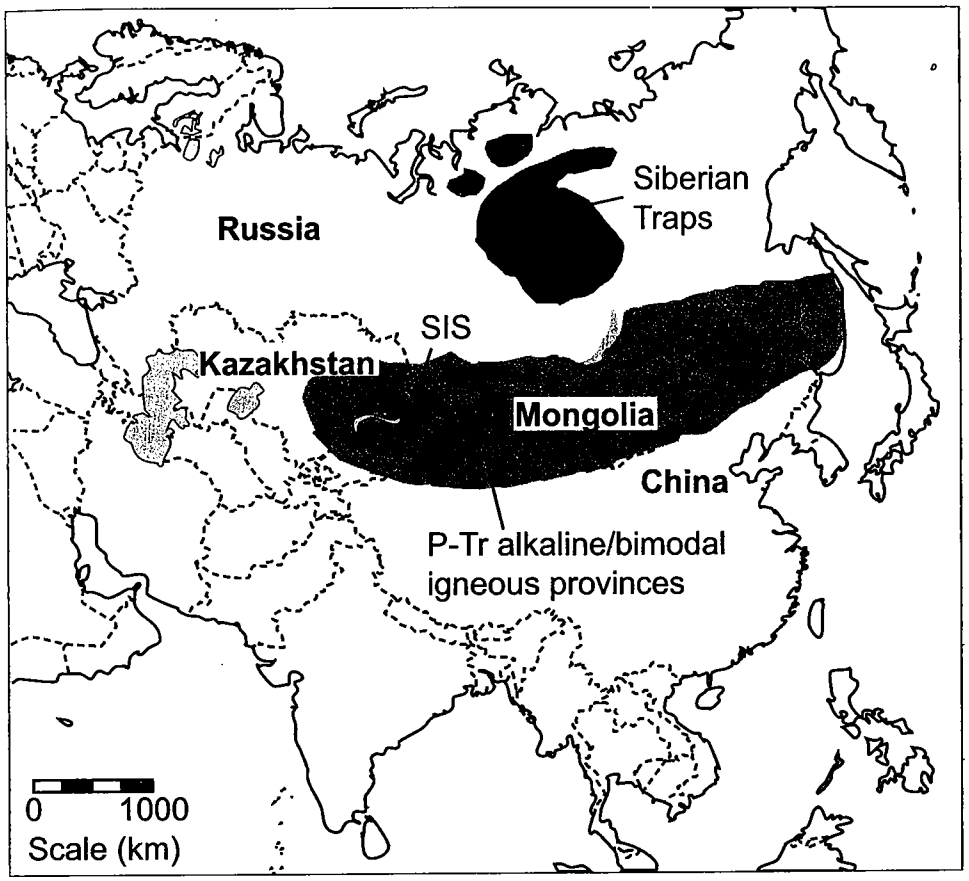

Figure 2. Map of Asia showing the locations of the SIS, the Siberian Traps, and the region of alkaline and bimodal igneous provinces hypothesized to be contemporaneous [*Dobretsov*, 1997].

hypothesis. If it is found that the Siberian Traps were associated with more distant alkaline/bimodal eruptions, that association will be an important constraint on any mechanism to explain the initiation and eruption of the Siberian Traps. The SIS, located ~1500 km southwest of the Siberian Traps, is one candidate for an igneous event that might be linked to their eruption, so we undertook $^{40}Ar/^{39}Ar$ experiments to examine that possibility.

2. Geologic Background

2.1. SIS Geology

[6] The Semeitau igneous series is a deeply eroded volcanic structure that outcrops in a series of low hills 45 km southwest of Semey (formerly Semipalatinsk), Kazakstan (Figure 1). The arcuate volcanic outcrop extends for ~50 km and consists of alkaline basaltic lavas, trachytic lavas, rhyolitic lavas, rhyolitic ash flows, and subvolcanic monzonites, syenites, granosyenites, and granites (Figure 3). Previous efforts to date the SIS include a paleontological assignment of early Triassic [*Istomin and Salmeneva*, 1964] and a Rb/Sr age of 254 ± 9 Ma [*Izokh*, 1983].

[7] Earlier work on the SIS comprised field mapping and petrologic analysis [*Izokh*, 1983; *Ermolov and Izokh*, 1977] and minor magnetic and gravity surveys [*Izokh*, 1983], all published in the Soviet literature (a few of which have been translated into English). A considerable number of exploratory boreholes were drilled to aid in locating suitable rock for road construction.

[8] On the basis of their own petrologic work and the field maps of previous studies, *Ermolov and Izokh* [1977] determined the following eruptive/intrusive history, from oldest to youngest: (1) alkaline basalt flows; (2) monzonites and monzonite porphyries; (3) trachyte extrusives, syenite and granosyenite porphyry intrusives; (4) rhyolite lavas, rhyolite ash flows, and granite porphyries; (5) leucocratic granites; and (6) diabase intrusives. Geochemical analyses indicate that the earliest basalts were the result of melting in the upper mantle, whereas the later silicic igneous units were the result of melting of the lower crust and progressive mixing of the crustal and mantle melts [*Ermolov and Izokh*, 1977].

2.2. Regional Geology

[9] Although eastern Kazakstan was still a deforming margin into the early Permian, the early Triassic to Recent geology of the region suggests tectonic quiescence. The SIS units are mapped as crosscutting thrusts that accommodated deformation of surrounding Carboniferous accretionary marine sedimentary and volcanoclastic rocks (Figure 1). This indicates that collisional deformation had probably ended before eruption of the SIS. Large chemical differences between the SIS rocks and the subduction-related magmatic bodies also demonstrate that the SIS was postcollisional [*Ermolov and Izokh*, 1977; *Berzin et al.*, 1994]. Since the eruption of the SIS, there was minor subsidence-related extension in the area, as evidenced by the opening of the Zaisan Basin. However, even though the SIS is overlain in

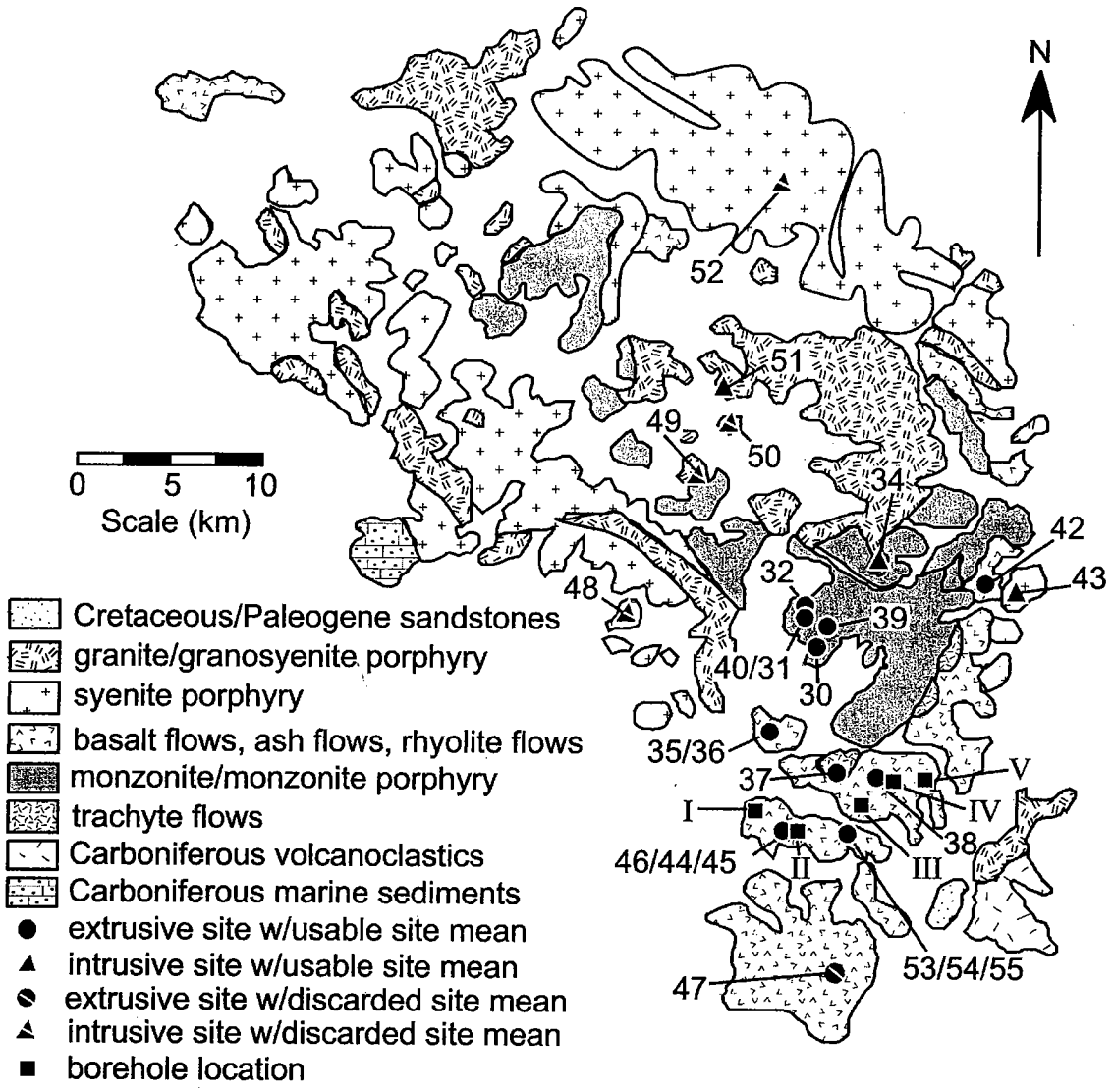

Figure 3. Geologic sketch map of the SIS [after *Ermolov and Izokh*, 1977], showing the outcrops of intrusive and extrusive lithologies, the locations of sites listed in Table 1, and locations of the boreholes shown in Figure 7. For the site numbers a slash indicates a locality in which the site after the slash immediately overlies the site before the slash.

one small locality by subhorizontally bedded Cretaceous-Paleogene sandstones [*Borovikov*, 1968; *Ermolov and Izokh*, 1977], there is no evidence for deep burial or major orogenic uplift of the complex [*Krestnikov and Reysner*, 1967].

3. Methods

3.1. Paleomagnetic Methodology

[10] We collected 331 oriented samples from 27 sites around the SIS, taking all samples by means of a gas-powered drill and orienting them using a magnetic compass and clinometer. Each site comprises a single outcrop of an individual lithology on a hill slope, stream bottom, or quarry wall. We generally avoided areas of high relief to minimize the possible effects of lightning, and we used Sun azimuths at each site to remove the effects of local magnetic anomalies. In an attempt to determine ancient horizontal at the time of eruption, we estimated structural attitudes for some of the extrusive sites using an average of several measurements of eutaxitic textures and, in a few cases, measurements of local contacts between extrusive units (Table 1).

[11] We measured remanent magnetizations with a Geofyzika JR-5 spinner magnetometer and a 2G horizontal access cryogenic magnetometer and stepwise demagnetized all samples discussed in this paper. We performed alternating field (AF) demagnetization to peak fields of 60–200 mT using a Sapphire SI-2 nonrotating AF demagnetizer and thermal demagnetization in air to temperatures of 550° to 650°C in a custom-built quasi-field-free (<12 gamma) furnace.

[12] In almost all cases, we determined the components of magnetization by fitting lines to the demagnetization data according to the technique of *Kirschvink* [1980]. Six sample demagnetization paths displayed unresolved multiple com-

Table 1. Paleomagnetic Site Data[a]

Site	Lithology	Emplacement	Thickness[b]	Attitude[c]	N/N_0	D	I	κ	α_{95}	Comments
46	basalt lava	extrusive	>5 m	...	5/5	232	−58	547.7	3.3	immediately underlies 45
37	trachyte lava	extrusive	...	...	9/9	227	−72	503.0	2.3	
30	monzonite	intrusive	...	...	8/8	250	−73	388.8	2.8	coarse-grained equigranular texture
32	monzonite porphyry	extrusive/intrusive	...	...	10/15	211	−79	359.4	2.6	fine-grained/glassy groundmass
31	monzonite	extrusive/intrusive	...	...	8/11	203	−80	555.6	2.4	fine-grained texture
40	monzonite	intrusive	...	...	8/8	193	−82	2227.3	1.1	coarse-grained equigranular texture
35	layered vitrophyre	extrusive	(3 m)	350 < 10[c]	13/13	236	−63	338.3	2.5	two layers, identical directions
38	layered vitrophyre	extrusive	(15 m)	80 < 50[d]	8/8	258	−59	22.0	12.0	steep dips: see text
44	vitrophyre	extrusive	5 m	219 < 19[c]	8/8	252	−60	169.1	4.3	$FeTiO_3$ CRM on top of magnetite TRM
53a	vitrophyre	extrusive	3 m	70 < 25[c]	4/4	223	−64.7	2347.6	1.9	immediately adjacent to site 53b
53b	rhyolite lava	extrusive	>3 m	70 < 25[c]	6/6	245	−49	66.2	8.3	
54	vitrophyre	extrusive	3 m	63 < 23[c]	9/9	237	−64	677.4	2.0	≈50 m from 53a, presumably same unit
42	ignimbrite	extrusive	10 m	200 < 13[c]	8/9	255	−71	547.2	2.4	<0.5 km from site 43 (syenite)
55	ignimbrite	extrusive	4 m	67 < 27[c]	5/6	233	−64	183.3	5.7	immediately overlies vitrophyre of 54
36	rhyolite lava	extrusive	4 m	355 < 10[c]	7/7	233	−74	179.2	4.9	immediately overlies 35
45	rhyolite lava	extrusive	5 m	219 < 19[c]	7/7	232	−54	103.8	6.0	immediately overlies 44
47	rhyolite lava	extrusive	15 m	variable	0/10	220	−63	122.8	6.3	severe normal polarity overprint (rejected)
34	granite porphyry	intrusive	...	...	6/12	251	−70	2177.8	1.5	6 IRM overprinted samples
49	granite porphyry	intrusive	...	...	0/8	R	R	13.6	180.0	unstable demagnetizations (rejected)
50	granite porphyry	intrusive	...	...	0/3	R	R	173.3	37.7	unstable demagnetizations (rejected)
	mafic xenoliths	inclusions in granite	1–30 cm	...	0/8	N	N	...	...	unstable, suspicion of overprint (rejected)
51	granite porphyry	intrusive	...	...	6/7	250	−78	163.9	5.2	minor high temperature component
52	syenite porphyry	intrusive	>50 m	...	0/5	MXD	MXD	...	57.2	unstable demagnetizations
43	syenite porphyry	intrusive	>50 m	...	9/12	30	70	22.1	11.2	(rejected)
48	syenite porphyry	intrusive	...	...	0/9	R	R	83.8	26.0	severely overprinted (rejected)
39	diabase dike	fine-grained intrusive	(3 m)	...	6/6	77	76	76.7	7.7	intrudes between monzonites of 30 and 40

[a]Geologic and remanence data for the 25 sites analyzed from the SIS, arranged in order of geologically inferred age (oldest at top, see text). Sites are composed of a single lithology at a single outcrop, some of which possess the same structural attitude. Emplacement is inferred from petrography and field data. N/N_0 is the ratio of samples used for a site mean to the total number of samples measured for that site. D and I are declination and inclination in geographic (in situ) coordinates. For sites where determination of a site mean was impossible, polarity is indicated as reverse (R), normal (N), or mixed (MXD); κ is the precision parameter and α_{95} is the angle of 95% confidence; see text for definitions. Rejection of a site mean is indicated in the comments; see text for discussion of rejected site means.

[b]Unit thicknesses are approximate except where in parentheses, indicating that an upper and lower contact made an exact measurement possible.

[c]Attitudes are listed as "downdip azimuth less than dip."

[d]Attitude was taken on eutaxitic texture.

ponents, necessitating the use of great circle demagnetization paths. *Fisher* [1953] statistics, as modified by *McFadden and McElhinny* [1988] for including great circle demagnetization data, were used to determine within-site means and overall means for the SIS. Circles of confidence about all calculated mean directions and poles are for $P = 0.05$, or 95% confidence, and are stated as α_{95} or A_{95} confidence intervals, respectively. We determined tectonic translations and rotations using the pole space equations of *Butler* [1992].

[13] We also performed low-field susceptibility versus temperature (K-T) experiments using powdered samples in argon in a Geofyzika KLY-2 kappabridge with a CS-2 high-temperature apparatus and measured anisotropy of magnetic susceptibility using the 15 position rotation scheme in a Geofyzika KLY-2 kappabridge or the three-position scheme in an AGICO KLY-3S kappabridge with rotating sample handler. We determined Curie temperatures from the K-T curves using the technique described by *Prévot et al.*, [1983]; these determinations are accurate within ±10°C.

3.2. The $^{40}Ar/^{39}Ar$ Methodology

[14] Two of the volcanic rocks, a vitrophyre (site 35) and a trachyte (site 37), appeared especially suitable for $^{40}Ar/^{39}Ar$ dating. Both of these contain large phenocrysts (up to 1 cm maximum dimension) of sanidine, which were easily separated by crushing and hand picking. Sanidine crystals from the 20–40 mesh fraction were ultrasonically rinsed in 7% HF for 5 min. Several grains from each sample were then coirradiated with the 28.02 Ma neutron fluence monitor Fish Canyon sanidine [*Renne et al.*, 1998] in the CLICIT facility of the Oregon State University TRIGA reactor for 20 hours. Standards were irradiated in the same wells in Al disks as were the samples, eliminating uncertainties due to possible

neutron fluence gradients. Single grains of each sample were degassed by incremental heating with a CO_2 laser using methods described by *Renne et al.* [1997].

4. Results

4.1. Paleomagnetic Results

[15] We determined paleomagnetic remanence directions for 213 samples from 25 of the 27 sites; two sites were redundant and therefore not measured. We determined within-site mean remanence directions ("site means") for 20 of these 25 sites (Table 1). Because of severe overprinting or large (>15°) within-site scatter, we did not determine site means for the other five sites.

[16] In the determination of the 20 usable site means, we discarded 20 of the 170 samples due to presumed large orientation errors (6 samples), unremovable isothermal remanent magnetization (IRM) overprints (8 samples), or unstable demagnetization paths (6 samples). Orientation errors were invoked only for samples that had broken out of the outcrop before orientation and possessed a remanence direction more than three standard deviations away from the mean remanence direction for its site. IRM overprints, probably lightning-induced, were recognized through a combination of high natural remanent magnetization (NRM) intensity, anomalous remanence direction, and a significant drop in NRM intensity at low (5–10 mT) applied alternating fields. Unstable demagnetization paths were those with repeated large and seemingly random changes in both declination and inclination or those with increases in intensity as temperature or alternating field increased near the end of demagnetization of the sample.

4.1.1. Extrusive igneous rocks

[17] We sampled 13 sites of extrusive rocks ranging in composition from mafic alkaline basalts and trachytes to silicic rhyolite lava flows and ash flows (ignimbrites and vitrophyres). Despite their age, most of these extrusives appear fresh and are stable and reliable paleomagnetic recorders. For 12 of these 13 sites, demagnetization behavior was straightforward, within-site dispersion is low, and the rock magnetic data indicate that titanomagnetite dominates the magnetic mineralogy. In the following discussion, the extrusive sites are divided into three groups according to their magnetic behavior, as the behavior in each group is consistent across lithology.

[18] Sample magnetization data from sites 35, 36, 37, 38, 42, 53a, 53b, 54, and 55 are characterized by high stability components of magnetization that, after removal of minor secondary overprints, decayed linearly toward the origin during AF and thermal demagnetization (Figures 4a–4b). Both demagnetization techniques yielded similar directions in those samples for which both techniques were used. Some sample data show consistent low-stability secondary components with a direction of north and down (Figure 4b), whereas others show overprints of no consistent direction. The former overprint direction is almost certainly of viscous origin, the latter may be minor isothermal remanence acquired from exposure to moderately strong fields due to lightning or unknown sources during sampling, shipping, and preparation. In a few cases, a high-intensity, low-coercivity overprint (probably a lightning-induced IRM) was present in the magnetization and could only be

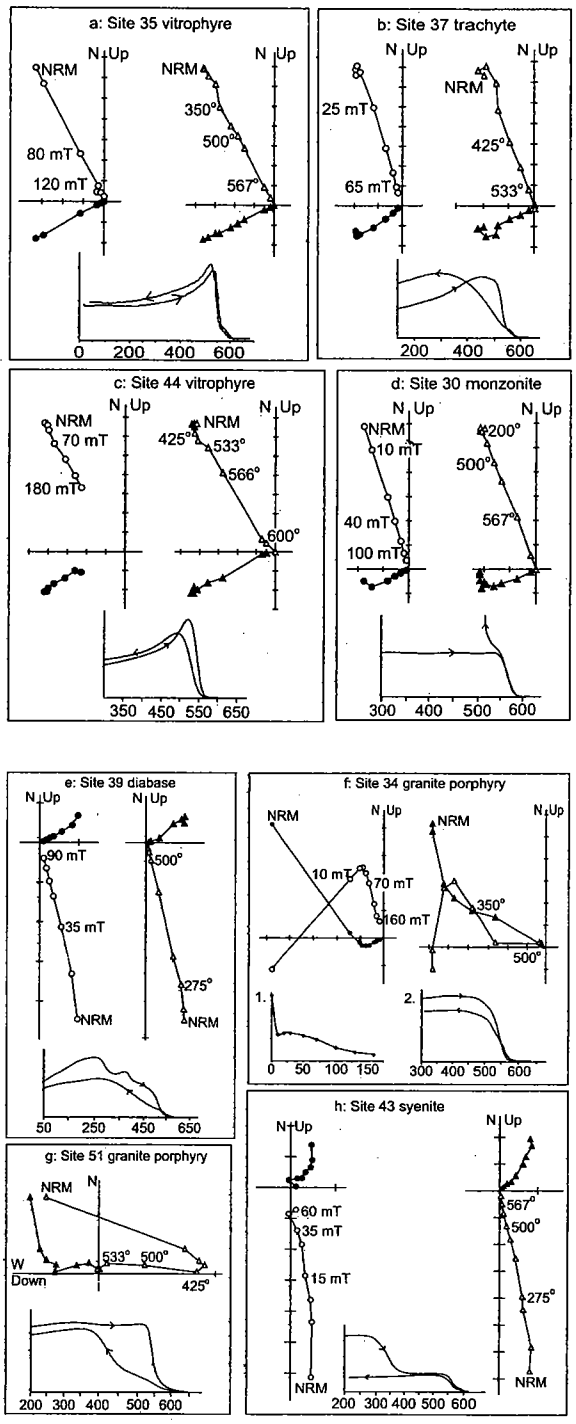

Figure 4. Representative orthogonal vector plots of alternating field (AF) and thermal demagnetization data and plots of data from low-field susceptibility versus temperature (K-T) experiments. On the orthogonal vector plots, circles indicate AF demagnetization data, triangles indicate thermal demagnetization data, solid symbols are the horizontal (declination) component, and open symbols are the vertical (inclination) component. On the K-T plots the abscissa is temperature in degrees Celsius, and the ordinate is susceptibility. Arrows indicate heating and cooling paths. Also shown in Figure 4f (bottom left) is a normalized intensity (ordinate) versus applied alternating field in mT (abscissa) for AF demagnetization.

Table 2. Rock Magnetic Data[a]

Site	Lithology	J_{NRM}	MDF	T_C	T_I
46	basalt lava	1.02	50	570[b]	150–375
37	trachyte lava	0.17	35	520,560	...
30	monzonite	0.35	30	570	...
32	monzonite	3.42	25	540	...
31	monzonite	1.09	25	540	...
40	monzonite	2.05	30	525	...
35	vitrophyre	5.26	75	560,580	...
38	vitrophyre	9.69	80	550,580	...
44	vitrophyre	8.77	180	545[b]	...
53a	vitrophyre	4.64	87	560	...
53b	rhyolite flow	1.81	45	570,610[b]	...
54	vitrophyre	7.17	80	565	...
42	ignimbrite	0.06	30	550	...
55	ignimbrite	1.27	20	535	...
36	rhyolite lava	0.29	40	540	...
45	rhyolite lava	0.78	80	550,610[b]	...
47	rhyolite lava	0.76	6	535	...
34	granite porphyry	2.05	...	545	...
49	granite porphyry	0.02	...	560	150–375
50	granite porphyry	0.02	30	560	...
51	granite porphyry	0.13	20	545	...
52	syenite porphyry	0.12	13	570	150–375
43	syenite porphyry	0.10	20	570	150–400
48	syenite porphyry	0.62	15	570,620	150–400
39	diabase dike	8.56	25	520	150–420

[a]Rock magnetic data for each paleomagnetic site listed in Table 1. J_{NRM} is NRM magnetization intensity, in A/m, MDF is median destructive field, in mT, T_C are Curie temperatures, determined from K-T experiments (see text), and T_I, where applicable, is the temperature range over which the titanomaghemite inverts.

[b]Samples that, during thermal demagnetization, retain 10–40 % of their magnetization above 600°C (see text).

removed with AF demagnetization. Although demagnetization effectively isolated a characteristic component in most samples, it failed to entirely remove the secondary overprints in four samples. These overprinted magnetizations nonetheless followed stable great circle paths toward directions that agree closely with the stable endpoint magnetizations for their respective sites, and therefore we included these data in the site means.

[19] The magnetic mineralogy of these well-behaved samples is dominated by unaltered Ti-poor titanomagnetite, as indicated by primary Curie temperatures ranging from 520°C to 570°C and median destructive fields (MDF) ranging from 20 to 87 mT (Table 2). Samples from some sites (Table 2) show a second drop in their K-T curves (i.e., Figures 4a and 4b) that suggests a second population of more iron-rich titanomagnetite. In the case of the samples from site 53b, this higher-temperature phase may be maghemite, as the Curie temperature is too high for magnetite and the irreversible drop in the K-T curve (not shown) is far too large to be explained by ilmenohematite, given that these samples were demagnetized by moderate alternating field (MDF = 45 mT). Also, other studies [*McIntosh*, 1991; *Palmer et al.*, 1996] of welded ash flows have observed similar behavior that after more extensive rock magnetic experiments, they attribute to maghemite that is stabilized against inversion by impurities in the lattice [*Dunlop and Ozdemir*, 1997]. In our samples this presumed maghemite carried the same remanence direction as the titanomagnetite, consistent with formation by deuteric oxidation during primary cooling.

[20] The second group of extrusive samples (sites 44, 45, and 46) is from a single locality and shows demagnetization behavior similar to the first group but with evidence of a minor chemical remanent magnetization (CRM) acquired after primary cooling. These samples display high MDFs (up to 180 mT), maximum unblocking temperatures of 640°C, and K-T Curie temperatures between 545°C and 610°C (Table 2). AF demagnetization of NRM decays linearly but does not reach the origin. Thermal demagnetization plots display a large linear segment up to 566°C that would miss the origin, followed by a smaller one ending at the origin around 640°C (Figure 4c). The direction indicated by the linear segment below 566°C agrees with the characteristic remanent magnetization (ChRM) directions measured in the first group of extrusives, whereas the 566°C–640°C component possessed a direction that is west-northwest and slightly shallower. Because of the high coercivity, high maximum unblocking temperature, and slightly different direction of this latter component, we interpret it as CRM carried by secondary ilmenohematite that probably formed in this one locality after acquisition of the thermoremanent magnetization (TRM). We take the large, lower-temperature component as the original TRM to use in our mean for the complex.

[21] The final group of extrusive data comes from one rhyolite flow (site 47) and consists of sample magnetizations with severe normal polarity overprints. Only one out of 10 sample magnetizations from this site attained a stable endpoint, whereas the remainder trended along short great circles toward expected reverse directions (Figure 5a) before becoming unstable above 500°C (not shown). Curie temperatures around 535°C indicate that the primary carrier of remanence is titanomagnetite, and the abnormally low MDFs (6 mT) may be the reason that these samples could be so badly overprinted. Because the mean for this site was

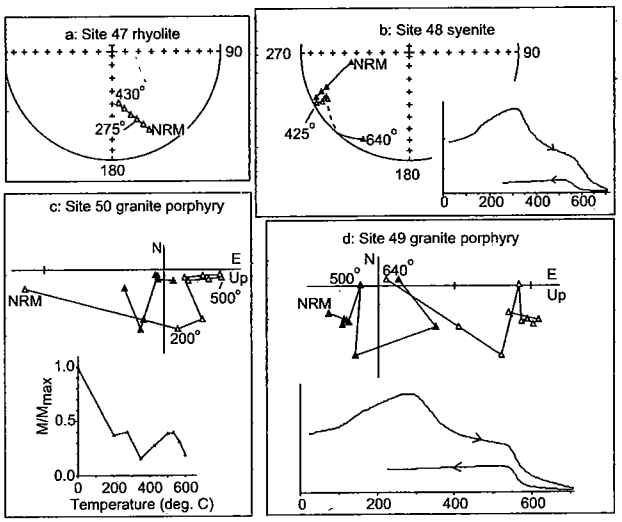

Figure 5. Representative (a–b) stereoplots and (c–d) orthogonal vector plots of thermal demagnetization data for sites with samples that were severely overprinted or have unacceptable scatter. A normalized intensity versus step plot is also shown for Figure 5c. On the stereoplots, solid symbols are lower hemisphere projections, and open symbols are upper hemisphere projections. Figures 5c and 5d are the same as described in Figure 4. See text for discussion of the plots and their unacceptable behavior.

determined primarily with poor quality great circles, we excluded it from consideration for the mean pole.

[22] We measured the anisotropy of magnetic susceptibility of most samples from the extrusive sites. The low overall anisotropy (K_{max}/K_{min} = 1.001 to 1.05) indicates that primary flow fabrics or other preferential orientations of the magnetic minerals probably had little effect on remanence direction. K_{max} directions, often interpreted as the direction of flow [e.g., *Palmer et al.*, 1996], are oriented along a north-northwest/south-southeast axis, but because they dip in both directions, they offer no indication whether the volcanic source was to the northwest or to the southeast. Given the pattern of lithologic units in the SIS (Figure 3), it seems geologically most reasonable that the source was to the north of the sites.

4.1.2. Intrusives

[23] The subvolcanic intrusives vary more than the extrusives in their rock magnetic properties and therefore in their stability during demagnetization. While some of the intrusives were as stable during demagnetization as the first group of extrusives described above, others had unstable magnetizations, showed rock magnetic evidence for severe alteration, and yielded poor data. The intrusive lithologies also divide into three groups based on their demagnetization behavior and their inferred magnetic mineralogy.

[24] The most easily interpretable demagnetization data are from the four sites of monzonites (sites 30, 31, 32, and 40), the granite porphyries (site 34), and the diabase dike (site 39). Overprints, sometimes similar to the present Earth's field direction, were removed at lower AF fields and temperatures, after which the sample magnetizations usually decayed linearly toward the origin (e.g., Figures 4d–4f). Thermal and AF demagnetization gave similar results, except when IRM overprints rendered thermal demagnetization ineffective (e.g., Figure 4f).

[25] Most of the samples in this group show MDFs between 25 and 30 mT and Curie temperatures between 520°C and 570°C, suggesting that unaltered titanomagnetite is the primary remanence carrier in these samples. Minor titanomaghemite is probably also present in the diabase dike of site 39, as demonstrated by the K-T curves in Figure 4e. This behavior is consistent with titanomaghemite [*Dunlop and Ozdemir*, 1997, Figure 3.12], in which the prominent drop in susceptibility beginning around 250°C indicates inversion to ilmenite-magnetite intergrowths. The successful removal of a lower-temperature component followed by the ChRM with a different, internally consistent direction at higher blocking temperatures suggests that titanomagnetite retains the primary TRM.

[26] Sites 30, 31, 32, and 40 (Table 1) come from different parts of a single laccolith [*Ermolov and Izokh*, 1977, and references therein] composed of several cooling units. We could not distinguish the different units in the field, but thin-section analysis revealed both coarse-grained equigranular (sites 30 and 40) and fine-grained porphyritic (sites 31 and 32) lithologies, suggesting units with different emplacement styles. The difference in remanence directions corroborates these observations because whereas the fine-grained sites 31 and 32 are indistinguishable at 95% confidence, the coarser-grained units (sites 30 and 40) differ both from each other and from 31 and 32. Moreover, although the coarse-grained texture indicates slower cooling times for sites 30 and 40, the 14° difference in remanence directions suggests that these directions are short-term averages at times of significantly different geomagnetic field direction.

[27] The second group consists of samples from a single site of granite porphyry that have a principal Curie point and MDF indicative of Fe-rich titanomagnetite (Table 2). Demagnetization data indicate the presence of a low-temperature viscous component directed north and down, followed by a large intermediate (425°C–533°C) component that is southwest and up and a small high-temperature (533°C–566°C) component that is directed northwest and up (Figure 4g). We interpret the intermediate component to be the primary TRM because its unblocking range is consistent with that of unaltered titanomagnetite. The anomalously directed high-temperature component is present only near to and above the titanomagnetite Curie temperature determined for these samples (545°C). Therefore this >533°C component is probably not a TRM but rather a minor secondary CRM perhaps carried by ilmenohematite. Because thermal demagnetization separated this presumed CRM cleanly from the TRM, we include the latter for our SIS mean.

[28] The five sites of weathered syenite porphyries (sites 43, 48, and 52) and granite porphyries (sites 49 and 50) constitute the third, most poorly behaving group of sites. Only one of them (site 43) yielded useful data because the majority of samples from the other sites were unstable or heavily overprinted.

[29] In the one site that yielded usable data (site 43), thermal demagnetization effectively removed the secondary overprint by 425°C and yielded a linear high-temperature component (Figure 4h). Although AF demagnetization gave roughly similar results, we do not consider these data as reliable because the highest-coercivity steps are scattered. For the other four sites, thermal demagnetization up to 640°C was performed with little success. While each of these four rejected sites includes one to two samples that decayed linearly to a reasonable reverse direction, the remainder suffered from severe overprinting possibly of present field origin (Figure 5b), unstable and erratic demagnetization paths (Figures 5c and 5d), or sudden gains in intensity at increasing temperatures (Figure 5c).

[30] Rock magnetic data indicate the presence of titanomagnetite and secondary titanomaghemite in these samples. K-T curves display an irreversible drop in susceptibility between 250°C and 380°C and a second and usually smaller drop beginning between 540°C and 580°C. We interpret the first drop as the inversion of secondary titanomaghemite to ilmenite and magnetite and the second drop as the Curie temperature of the primary titanomagnetite. In the case of site 48 the second drop in the K-T curves indicates a Curie temperature of 620°C (Table 2 and Figure 5b), suggesting the additional presence of ilmenohematite in these samples.

[31] Although the presence of secondary titanomaghemite does not necessarily explain the unstable behavior of the rejected sample magnetizations (Table 1), it may explain why sample magnetizations from site 43 behaved differently during AF and thermal demagnetization. For these samples, thermal demagnetization yielded linear high-temperature components because heating had destroyed the titanomaghemite and its secondary remanence well before the titanomagnetite had completely unblocked (Figure 4h). AF demagnetization, by contrast, could not separate the titano-

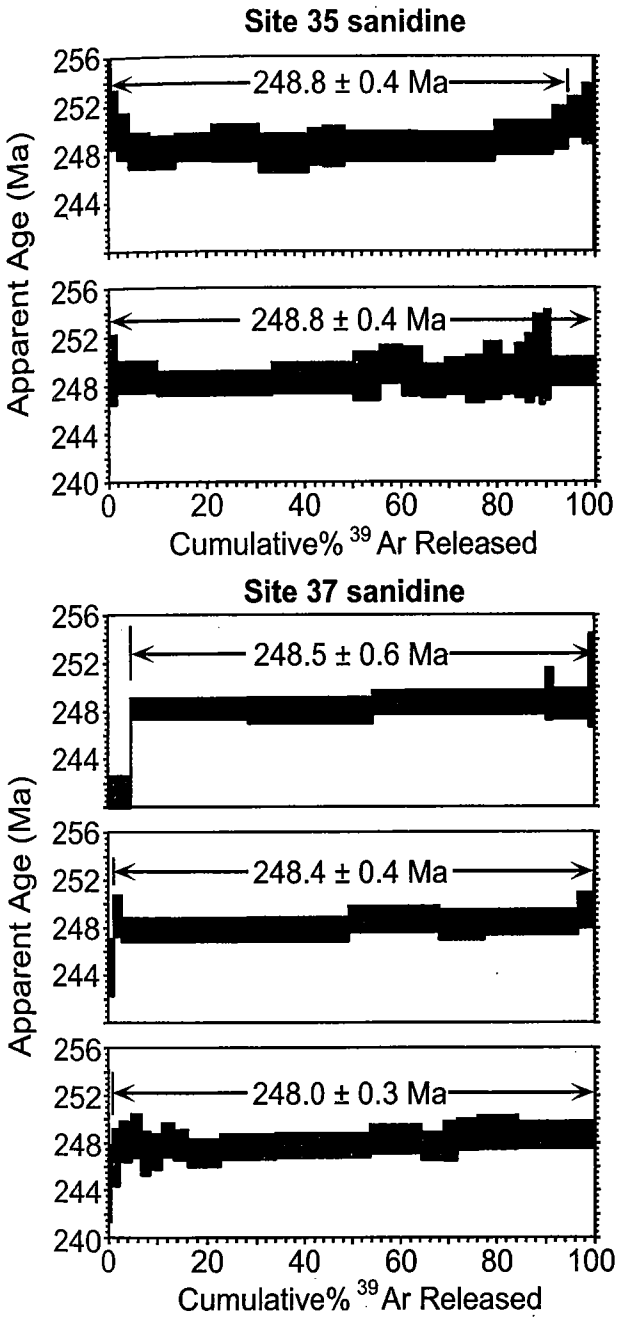

Figure 6. Laser step-heating diagrams for five single-crystal $^{40}Ar/^{39}Ar$ age determinations from sites 35 and 37. See text for discussion of methods and data analysis.

maghemite and titanomagnetite components because these minerals have roughly similar coercivities and therefore demagnetized simultaneously, potentially yielding more scattered results.

4.2. The $^{40}Ar/^{39}Ar$ Results

[32] Two sanidine crystals from the vitrophyre of site 35 yielded age plateaus for ~95% and 100% of the ^{39}Ar released (Figure 6), with indistinguishable plateau ages (error-weighted mean of all plateau steps) of 248.8 ± 0.4 Ma (2σ analytical errors neglecting systematic error contributions from decay constants and standards). Combining all plateau steps and hierarchically propagating [*Renne et al.*, 1996] the 0.18% analytical error in determining neutron fluence for this sample yields a plateau age of 248.8 ± 0.5 Ma, which is taken to reflect the eruption age of this unit. Three sanidine crystals from the trachyte of site 37 yielded plateaus over >95% of the ^{39}Ar released, with mutually indistinguishable plateau ages of 248.5 ± 0.6, 248.4 ± 0.4, and 248.0 ± 0.3 Ma. The weighted mean of these three plateau ages, including the ±0.21% neutron fluence determination as above, is 248.2 ± 0.5 Ma, interpreted as the eruption age of this unit. Tables of the complete analytical data for all samples are available in the data supplement to this article.[1]

[33] The ages inferred for sites 35 and 37 are indistinguishable at 95% confidence, differing by only 0.6 ± 0.7 Ma. These ages may be compared straightforwardly with $^{40}Ar/^{39}Ar$ ages for the Siberian Traps reported by *Renne and Basu* [1991] and recalculated by *Renne et al.* [1995]. This comparison indicates that the SIS was active ~1.5 Myr later than the eruption of the Ivakinsky Suite, which is inferred to be among the earliest eruptions of the Siberian Traps. Note that due to systematic bias between current calibrations [e.g., *Min et al.*, 2000], the $^{40}Ar/^{39}Ar$ ages presented here cannot be compared directly with the U/Pb data of *Kamo et al.* [1996].

5. Discussion

[34] In determining our overall SIS mean direction and pole we chose to analyze 20 of the 25 measured site means. This choice was based on the criteria that an accepted site-mean α_{95} angle must be less than 15° and the majority of data used for determining that mean must be least squares lines. Sites that we excluded from consideration were severely overprinted (site 47) or have badly scattered directions, with α_{95} angles ranging from 26° to 180°. By contrast, the α_{95} of site-mean directions that we accepted are generally much lower: 1.1°–12°, with 13 of them <5°.

5.1. Paleomagnetic Stability

[35] Remanence data, $^{40}Ar/^{39}Ar$ data, and rock magnetic data all suggest that our SIS directions are primary early Triassic thermoremanent magnetizations. Although a fold test is impossible because of the lack of postcooling deformation, the presence of two units with opposite polarity from the rest (Table 1) indicates that large-scale remagnetization is unlikely, as such a remagnetization would impart a single polarity to all units. The $^{40}Ar/^{39}Ar$ experiments support this contention: Data from extrusives at sites 35 and 37 indicate that these rocks have not undergone significant reheating and hence release of argon since their time of eruption. Massive chemical remagnetization is also unlikely: Thin section observations indicate that the samples experienced only slight alteration, and rock magnetic observations on samples from the accepted sites indicate that the major carrier of remanence is unaltered titanomagnetite. Minor high-temperature phases carry remanence that usually agrees in direction with that of the titanomagnetite, consistent with an origin by deuteric oxidation during primary cooling. Although viscous overprinting was present in many sample

[1] Supporting material is available via Web browser or via Anonymous FTP from ftp://kosmos.agu.org, directory "apend" (Username = "anonymous", Password = "guest"); subdirectories in the ftp site are arranged by paper number. Information on searching and submitting electronic supplements is found at http://www.agu.org/pubs/esupp_about.html.

magnetizations, almost all samples yielded stable endpoint magnetization directions different from the overprint, demonstrating that thermal and AF demagnetization were effective. We discarded those data that show evidence of unremovable viscous, IRM, or chemical overprinting.

[36] Small-scale reheating remagnetization by shallow intrusive bodies is possible in caldera complexes such as the SIS [e.g., *Hagstrum and Lipman*, 1986], but in the case of the data for the SIS this is very unlikely. Given intrusion temperatures of 850°C–1200°C [*Izokh*, 1983], depths beneath extrusive cover (from boreholes), and approximate intrusion sizes [*Ermolov and Izokh*, 1977], the intrusions could not have reheated the sampled extrusives to sufficient temperatures to have completely remagnetized them. Using the above intrusion temperatures, simple heat flow calculations [*Jaeger*, 1968], and thermoviscous blocking diagrams of magnetite [*Pullaiah et al.*, 1975], we estimate that any intrusive reheating overprints would be removed by thermal demagnetization to 250°C–350°C. Mean ChRM directions for the extrusives corroborate the lack of reheating effects: Extrusive units in direct stratigraphic contact (sites 46/44/45, 53a/53b, and 35/36) have significantly different remanence directions, indicating they were not reheated as a group. We could not perform a similar analysis on the intrusive units, but in all areas in which we sampled intrusive bodies <1 km from other intrusive or extrusive sites (i.e., sites 30, 39, 40, 31/32, 42, and 43, see Figure 3), mean remanence directions are significantly different and sometimes of opposite polarity. This demonstrates that reheating by nearby intrusions probably did not overprint the remanence at the sites that we measured.

5.2. Structural Deformation

[37] *Ermolov and Izokh* [1977] stated that the SIS is relatively flat-lying and undeformed, and we confirmed their conclusion through examination of borehole data. Figure 7 shows representative borehole logs from which we correlated the boundaries between tuffaceous units and overlying welded vitrophyre/ignimbrite sequences; the locations of the boreholes are shown in Figure 3. Average dips between boreholes range from 1.5° to 2.5° and vary in direction from southwest to northwest to east-northeast. Because of the shallowness of these dips and inconsistency of dip directions, we conclude that the SIS has not been tilted significantly either at the scale of the sites or the entire complex. Therefore we interpreted and analyzed the site means in geographic coordinates. In situ between-site dispersion of the extrusives is only 9.5° (most of which is probably due to secular variation, as discussed below), supporting our contention that the effects of deformation are minor.

[38] In the field, we measured attitudes of eutaxitic textures and one layer contact; these are listed in Table 1. Dips range from 10° to 50° and disagree with the borehole data, meaning almost certainly that the local-scale eutaxitic textures and layer contacts do not represent paleohorizontal. Previous paleomagnetic studies of ash flows, particularly in Tertiary caldera complexes in the western United States, have noted increased between-site dispersion after structural correction, a result interpreted as indicating inaccurate representation of paleohorizontal by eutaxitic textures and welding breaks [*Grommé et al.*, 1972; *Geismann et al.*, 1982; *Hagstrum and Lipman*, 1986; *Hagstrum and Gans*,

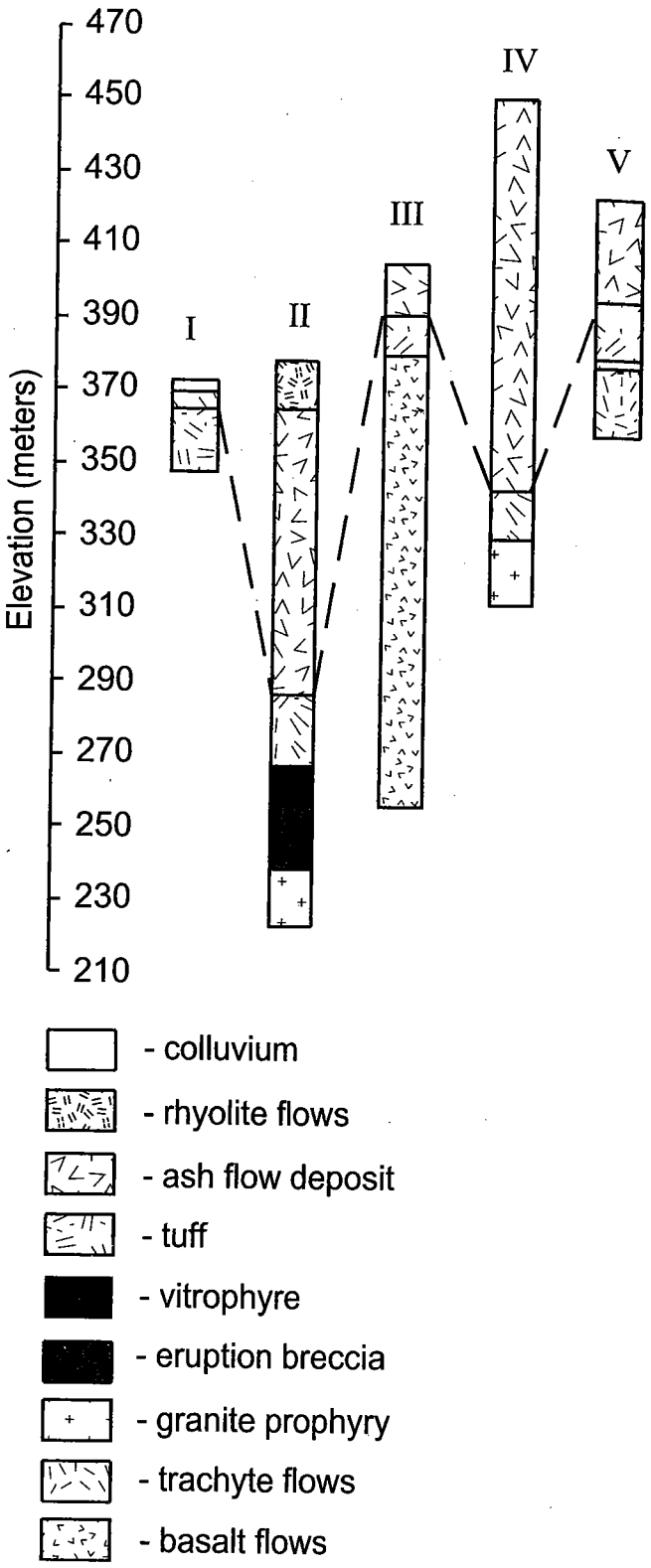

Figure 7. Borehole logs from the five localities indicated in Figure 3. Dashed lines are the unit correlations used for determinations of structural attitudes, indicating average dips of 2.5° or less (see text).

Table 3. Cooling Unit Data[a]

Cooling Unit	Lithology	Emplacement	N/N_0	D	I	κ	α_{95}	Plong	Plat	A_{95}
46	basalt flow	quick	5/5	232.0	−58.1	547.7	3.3	166.1	51.5	4.2
37	trachyte flow	quick	9/9	227.0	−71.6	503.0	2.3	138.5	61.8	3.8
30	monzonite	quick	8/8	250.3	−73.3	388.8	2.8	129.3	50.1	4.7
31/32	monzonite	quick	18/26	207.6	−79.4	417.2	1.7	103.7	66.6	3.2
40	monzonite	quick	8/8	193.4	−82.2	2227	1.1	87.9	64.8	2.1
35/53a/54/55	vitrophyre sequence	quick	31/32	234.3	−63.7	331.7	1.4	155.7	54	2.0
38/44	vitrophyre	quick	16/16	254.7	−59.6	38.7	6.0	149.9	38.8	7.8
53b	rhyolite flow	quick	6/6	245.3	−48.5	66.2	8.3	167.0	37.6	8.8
36	rhyolite flow	quick	7/7	233.3	−74.2	179.2	4.9	129.5	58.9	8.4
45	rhyolite flow	quick	7/7	232.2	−54.3	103.8	6.0	171.3	49.5	7.1
42	ignimbrite	quick	8/9	255.3	−71.4	547.2	2.4	131.5	46.6	3.9
34	granite porphyry	slow	6/12	251.0	−69.8	2178	1.5	136.2	47.9	2.4
51	granite porphyry	slow	6/7	249.5	−77.9	163.9	5.2	116.9	52.5	9.5
43	syenite porphyry	slow	9/12	30.1	70.3	22.1	11.2	144.7	71.2	18.0
39	diabase dike	quick	6/6	76.6	76.2	76.7	7.7	120.4	48.9	13.7

[a]Mean directions, north poles, and statistical data for cooling units used for determination of the SIS mean pole. Same as in Table 1 with the addition of Plat and Plong, the pole latitude and longitude, respectively.

1989; *McIntosh*, 1991]. Eutaxitic textures in ash flow deposits result from the flattening, compaction, and stretching of glass and pumice shards under gravitational loading during emplacement. Outcrop-scale eutaxitic textures may show initial dips resulting from emplacement of a flow on irregular topography [*McIntosh*, 1991], paleohill slopes [*Hagstrum and Gans*, 1989], or in paleostream channels [*Chapin and Lowell*, 1979]. Preremanence-blocking slump and creep of hot ash flows can also distort the eutaxitic textures away from paleohorizontal prior to TRM acquisition.

[39] The inaccuracy of our outcrop-scale estimates of paleohorizontal becomes particularly apparent when we apply them as structural corrections to the remanence measurements. For example, two groups of geographically separated vitrophyre sequences (site 35 and 53a/54/55) have nearly identical mean remanence directions in geographic coordinates, but using the attitudes in Table 1, their means scatter after structural correction (an apparent failure of the fold test). For all of the extrusive units, κ values decrease significantly when these structural corrections are applied ($\kappa_{geog} = 89.4$, $\kappa_{strat} = 12.4$). We showed in section 5.1 that remanence, rock magnetic, and argon-release data argue strongly against wholesale remagnetization. The evidence is clear that these eutaxitic textures are unreliable indicators of paleohorizontal; therefore it is incorrect to use them for a fold test.

5.3. Cooling Units

[40] When analyzing the site-mean results, we have taken into account the high probability that we sampled some of the same intrusive or extrusive cooling units at different sites. If we were to take two means sampled from the same cooling unit as discrete entities, the paleofield recorded in that unit would be statistically overrepresented. This is particularly a problem in the ignimbrite and vitrophyre sites, as singular ash flow cooling units can extend over thousands of square kilometers [*Lipman*, 1984]. For this reason, we assumed that samples from different sites are part of the same cooling unit when their site-mean directions are statistically indistinguishable and when it is geologically reasonable that they are part of the same unit. The samples from these sites we then averaged into a single cooling unit mean. For instance, the site 35 vitrophyre and sites 53a, 54, and 55 vitrophyre-ignimbrite sequences are not statistically distinguishable at 95% confidence [*Watson*, 1956], so we interpreted them as being the same cooling unit. Similarly, we combined the remaining two vitrophyre localities (sites 38 and 44) because they have insignificantly different directions. We consider them a second vitrophyre cooling unit because they do differ from the 35/53a/54/55 group at 95% confidence. The sample directions from sites 31 and 32 are also combined according to this scheme. These cooling unit data are listed in Table 3 and are shown in Figure 8.

5.4. Mean Paleomagnetic Direction and Pole

[41] To be valid for tectonic analysis, a paleomagnetic direction must be an average of data over a long enough

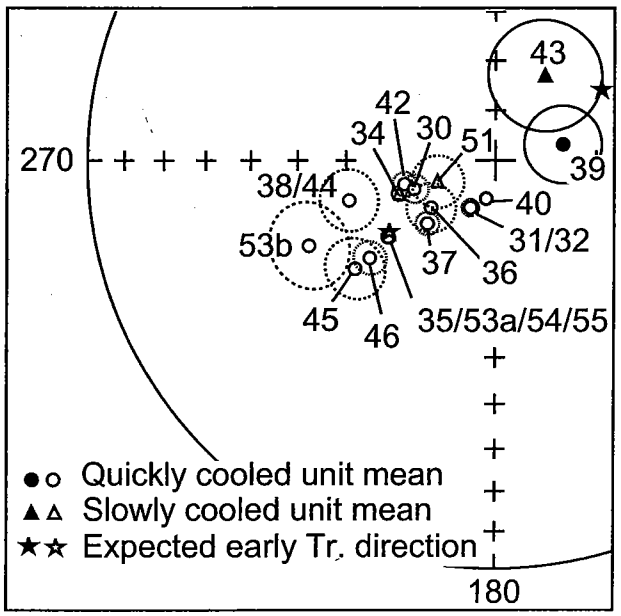

Figure 8. Equal-area net of the mean remanence directions and α_{95} circles for the 15 cooling units of the SIS, in geographic coordinates. Triangles indicate slowly cooled units, and circles indicate quickly cooled units. Solid symbols indicate lower hemisphere (normal) directions, and open symbols indicate upper hemisphere (reverse) directions. Stars indicate the expected Siberian lower Triassic direction [from *Smethurst et al.*, 1998].

Table 4. Averaging Scheme Results

Pole	N	D	I	κ	α_{95}
SIS mean	15	238.1	−69.4	51.6	5.4
Alternative 1	20	237.4	−68.8	56.2	4.4
Alternative 2	4	236.4	−72.3	122.4	8.3

period of secular variation to yield a good approximation of the ancient axial dipole field at the site. This period is thought generally to be of order 10 kyr [e.g., *Butler*, 1992]. With paleomagnetic recordings of 15 temporally spaced cooling units (Table 3 and Figure 8), including three subvolcanic intrusions that individually averaged secular variation to some degree, this study surely meets that requirement. That these cooling units span more than 10 kyr is clear because they represent three different periods of magma genesis of the SIS that entailed considerable petrologic evolution: the early (basalt and trachyte), middle (monzonite, rhyolite, ash flows and granite), and late (late granitoid and diabase) stages described by *Ermolov and Izokh* [1977]. A further indication that our data have sampled a long period of secular variation is the presence of both polarities. It is worth noting as well that the angular dispersion about the mean of these 15 cooling units that are 250 Ma in age is not different at the 95% confidence level from the average for secular variation estimated from lava flows erupted at the same latitude during the past 5 Myr [*Merrill et al.*, 1996].

[42] A strength of this study is the use of directions from different geographic locations, lithologies, and emplacement mechanisms. The scheme that we prefer for combining these various directions into an SIS mean maintains much of the variety of localities while still taking into account that we almost certainly sampled several of the units more than once at different localities. This method, which entails averaging 15 cooling units of equal weight, gives the N = 15 cooling unit average in Table 4 and yields the mean direction given in Table 5.

[43] An alternate averaging scheme is to simply average all 20 sites, taking no account of repeat sampling of cooling units (Table 4). This scheme optimizes averaging of errors specific to the locality and unit, such as jostling of outcrop, block rotations, and differing amounts of small but lingering overprints. However, this scheme ignores the strong probability that we repeat sampled some of the same cooling units, biasing the mean toward the directions of those units and artificially decreasing the confidence interval (because of the artificially larger N).

[44] Another alternative scheme would be to average the 12 quickly cooled units, assign unit weight to that mean, and then average it with the three most slowly cooled intrusive units. This scheme might be advantageous if the subvolcanic intrusive units cooled slowly enough to average secular variation and to recover the dipole field direction. The substantial difference in direction between the syenite porphyry and the two granite porphyries, however, shows that this is not the case (Table 3 and Figure 8). The much increased weighting of these three intrusive directions would bias the mean toward them, greatly limiting the averaging of undetected locality-specific errors.

[45] It is reassuring that the three different mean directions in Table 4 are separated by no more than 3.5° and differ from each other at a very low confidence level (26%), so the choice of scheme does not greatly influence the outcome. Because the alternate averaging schemes fail to account for the differences in cooling histories of the SIS units, we use the N = 15 averaging scheme for calculating the paleomagnetic pole (Table 5).

6. Tectonic Implications

6.1. Reference Pole

[46] For our tectonic analysis we chose the 248 Ma Siberian reference pole of *Smethurst et al.* [1998] because it comprises studies of known quality performed only on igneous rocks. Choosing a Siberian reference pole is difficult because demagnetization techniques and tests for magnetic stability for the reference data are often unpublished, rendering the quality of reference poles uncertain [*Van der Voo*, 1993]. The Smethurst et al. pole avoids this problem because demagnetization techniques and field tests are known and quality factors [*Van der Voo*, 1993] of 4 (two studies) and 5 (two studies) have been assigned for the data that constitute the pole. Our confidence in the pole is enhanced by comparison with a recent update of the Siberian reference pole (V. A. Kravchinsky, personal communication, 2001). The updated pole, determined using rocks related to the Siberian Traps, is statistically indistinguishable from that of Smethurst et al. and, in this study, yields the same tectonic interpretation. The Smethurst et al. pole is particularly appropriate for our analysis because it comprises only studies of igneous rocks of similar age to the SIS magnetization age of 248–249 Ma.

[47] Assuming that Europe and Siberia were tectonically coherent by the mid-Permian, *Van der Voo* [1993] proposed the use of better constrained European reference poles as a substitute for Siberian data, thereby circumventing the problems posed by poorly documented Russian data. Indeed, the early Triassic European reference pole [*Van der Voo*, 1993] is only 2.1° from the more recent Siberian pole [*Smethurst et al.*, 1998] discussed above, so either pole appears to be equally valid for the analysis. Both reference poles are listed in Table 5 and displayed in Figure 9.

6.2. Tectonic Analysis

[48] Our preferred SIS pole is statistically indistinguishable from the Siberian reference pole at 95% confidence,

Table 5. Paleomagnetic Poles[a]

Pole	D	I	α_{95}	Slat	Slong	Plat	Plong	N	K	A_{95}	Age	Reference
SIS	238	−69	5.4	50.1	79.6	56	139	15	24.6	7.9	248–249	1
Siberian Lower Triassic	...	...	...	...	...	53	153	4	49	10	248–249	2
European Lower Triassic	...	...	...	...	...	52	150	11	111.4	4	233–245	3

[a]Directional data, pole locations, and statistics for the SIS and pole location data for cratonal reference poles (see text). Slat and Slong are site latitude and longitude, respectively. References: 1, this study; 2, *Smethurst et al.* [1998]; 3, *Van der Voo* [1993].

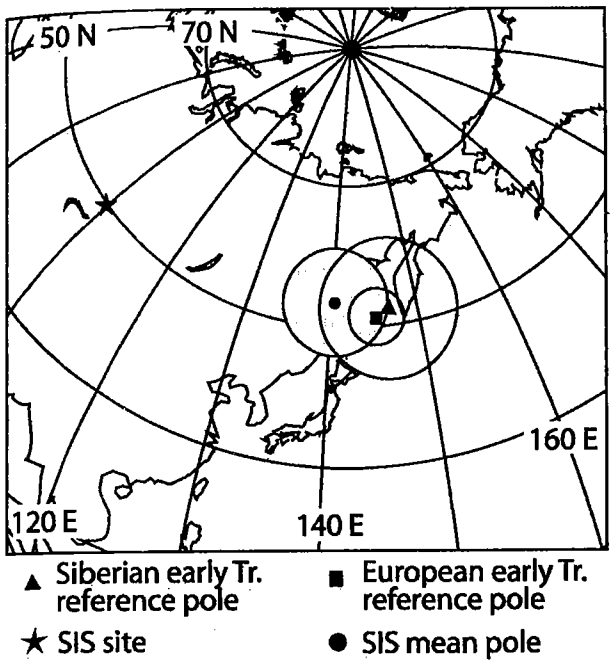

Figure 9. Schmidt projection showing the locations and A_{95} confidence circles for poles discussed in the text and listed in Table 5. Also shown are the SIS site location and outlines of the continents.

showing neither significant rotation (1° ± 16°) nor poleward translation (−8° ± 10°). This concordance of poles strongly supports previous arguments that Kazakstan and Siberia were joined by mid-Permian time [*Khramov*, 1982; *Zhao et al.*, 1990; *Bazhenov et al.*, 1999]. Prior to this study, paleomagnetic data supporting this hypothesis were too poorly documented, were of insufficient quality, or were from too limited a geographic region to effectively test this hypothesis. Our data, when combined with inclination data from the Tien Shan [*Bazhenov et al.*, 1999], are of sufficient quality and spatial extent to show that Kazakstan and Siberia were tectonically coherent by the early Mesozoic.

[49] Our data are not consistent with substantial clockwise rotation of Siberia relative to its margins [*Bazhenov and Mossakovsky*, 1986]. This is not a surprising result given the concordance of the most recent early Triassic paleomagnetic poles from Siberia and Europe discussed above. On the basis of paleomagnetic and geologic data, *Bazhenov and Mossakovsky* [1986] argued that beginning in the early Triassic, the Siberian craton rotated 12° clockwise relative to the eastern European craton. Although the comparison of the most recent paleomagnetic poles for Siberia [*Smethurst et al.*, 1998] and Europe [*Van der Voo*, 1993] reveals no significant relative rotations (3° ± 13°) between the two cratons, given the error intervals, the hypothesis of 12° of rotation of the Siberian craton cannot be ruled out with 95% confidence.

[50] *Allen et al.* [1995] suggested that a clockwise rotation of Siberia and its folded margin relative to the Russian craton and northwest China occurred in the late Permian to early Triassic, accommodated by left-lateral shear on the southeast-northwest trending Gornostaev, Irtysh, and Kalba-Chingiz shear zones. They cited the opening of the Junggar, Alakol, Turfan, and western Siberian basins as evidence for such motions, and they specifically ascribed the magmatism of the SIS, located on the north wall of the Gornostaev fault (Figure 1), as being the result of pull-apart extension on a left-stepping bend of a fault that they infer to be left lateral. Large left-lateral shear would be expected to cause local counterclockwise rotation of remanence directions within the shear zones relative to directions outside of the shear zones. Comparison of the SIS to the coeval European reference pole [*Van der Voo*, 1993] reveals no significant rotation, suggesting that there may have been little motion on the shear zone after magnetization of the SIS. This inference is actually consistent with the speculation of Allen et al., who suggested that the shear zones were locked after the early Triassic.

6.3. Relationship to Asian Permo-Triassic Magmatism

[51] The similarity of $^{40}Ar/^{39}Ar$ ages for the Siberian Traps and the SIS presented in this paper is striking; the 248–249 Ma SIS is very close to the 250.0 ± 1.6 Ma [*Renne et al.*, 1995] inception of the Siberian Traps section at Noril'sk. These data are consistent with the notion that the Siberian Traps and the SIS are genetically related, though, of course, they could be similar by chance.

[52] *Dobretsov* [1997] has suggested a single superplume or multiple genetically related plumes were the cause of both the Siberian Traps and the broad swath of alkaline/bimodal magmatism in central Asia. At this point, however, his hypothesis lacks sufficient supporting data and does not address seemingly contradictory geologic and tectonic evidence. For example, the eruption ages that he uses to relate the silicic/bimodal bodies to the Siberian Traps are largely K-Ar ages, which lack the precision necessary to support his hypothesis. Many of these silicic/bimodal rocks are emplaced on the Mongolia/North China block (Figure 2), most of which was several thousand kilometers from the southern Siberian margin in the early Mesozoic [e.g., *Zhao et al.*, 1990; *Enkin et al.*, 1992]. Also, recent articles [*Kamo et al.*, 1996; *Czamanske et al.*, 1998] strongly contend that the sedimentary record, cited as evidence for a plume (see *Dobretsov* [1997]; also speculated on by *Renne et al.* [1995]), does not show evidence of the broad uplift expected from the sublithospheric impact of a plume head.

[53] Despite the striking coincidence implied by the data that we present in this paper, it is too early in the close examination of Asian P-Tr magmatism to assume that many of the igneous bodies are genetically linked satellites of the Siberian Traps. Similar studies to this one on other igneous bodies, and geochemical fingerprinting as well, will provide a test of the idea of a common magmatic origin and shed light on the mechanism that generated Siberian Traps volcanism. We would expect distinct spatiotemporal patterns of magmatism (and uplift) for a single gigantic plume head that spread out under the lithosphere [e.g., *Campbell and Griffiths*, 1990], for multiple daughter plumes that independently impacted the lithosphere [*Dobretsov*, 1997], for a single plume source that fed both the Siberian Traps and far-flung eruptive centers by flow along sublithospheric channels [e.g., *Ebinger and Sleep*, 1998], or for nonplume mechanisms involving only shallow convection and decompression melting controlled by a step in the lithosphere [*King and Anderson*, 1998] or lithospheric thinning [*White and McKenzie*, 1989; *Elkins-Tanton and Hager*, 2000].

[54] The age data presented here are also noteworthy because they reveal silicic pyroclastic volcanism slightly younger than the main phase of basaltic Siberian Traps eruptions. This evolutionary sequence establishes a similarity to other continental flood basalt provinces, in which dominantly basaltic sequences are capped by later silicic flows that often betray a lithospheric genesis. Such a sequence is well-illustrated in the Paraná-Etendeka [*Hawkesworth et al.*, 1992] and Ethiopia-Yemen provinces [*Mohr and Zanettin*, 1988].

7. Conclusions

[55] We determined a paleomagnetic pole for the early Triassic Semeitau igneous series from directions of stable remanent magnetization of 150 samples taken in both intrusive and extrusive igneous rocks. These directions include both polarities and represent temporally spaced phases of eruption, and their ages are unusually well determined at 248–249 Ma. The Semeitau pole is located at 56°N, 139°E (N = 15, K = 24.6, A_{95} = 7.9) and is concordant with the coeval Siberian reference pole [*Smethurst et al.*, 1998]. The lack of significant translation (−8° ± 10°) and rotation (1° ± 16°) strongly supports post-Permian coherence of Kazakstan and Siberia and argues against large Triassic clockwise rotations of Siberia or large post-early Triassic shear motion in eastern Kazakstan.

[56] The $^{40}Ar/^{39}Ar$ dates of extrusives from the SIS indicate that the SIS erupted shortly after the main pulse of the Siberian Traps, supporting the hypothesis of a genetic relationship. High-precision geochronology of widely scattered igneous bodies similar to the SIS is necessary to further examine potential genetic relationships among these events.

[57] **Acknowledgments.** We thank Trond Torsvik, Jim Gill, Quentin Williams, and an anonymous reviewer for their helpful comments on this paper. We also gratefully acknowledge Randy Enkin, Jean-Pascal Cogné, Trond Torsvik, and Mark Smethurst for the use of their data analysis software. This work was funded by NSF grants EAR 97-06439 (awarded to R. S. Coe) and EAR-99-09517 (awarded to P. R. Renne).

References

Allen, M. B., A. M. C. Şengör, and B. A. Natal'in, Junggar, Turfan, and Alakol basins as late Permian to Early Triassic extensional structures in a sinistral shear zone in the Altaid orogenic collage, central Asia, *J. Geol. Soc. London*, *152*, 327–338, 1995.

Basu, A. R., R. J. Poreda, P. R. Renne, F. Teichmann, Y. Vasiliev, N. V. Sobolev, and B. D. Turrin, High ^{3}He plume origin and temporal-spatial evolution of the Siberian flood basalts, *Science*, *269*, 822–825, 1995.

Bazhenov, M. L., and A. A. Mossakovsky, Horizontal displacements of the Siberian platform in the Triassic, from the paleomagnetic data, *Geotectonics*, *20*, 40–47, 1986.

Bazhenov, M. L., V. L. Klishevich, and V. A. Tselmovich, Palaeomagnetism of Permian red beds from south Kazakstan; DRM inclination error or CRM shallowed directions?, *Geophys. J. Int.*, *120*, 445–452, 1995.

Bazhenov, M. L., V. S. Burtman, and A. V. Dvorova, Permian paleomagnetism of the Tien Shan fold belt, central Asia: Post-collisional rotations and deformation, *Tectonophysics*, *312*, 303–329, 1999.

Berzin, N. A., R. G. Coleman, N. L. Dobretsov, L. P. Zonenshain, X. Xiao, and E. Z. Chang, Geodynamic map of the western part of the Paleoasian Ocean, *Russ. Geol. Geophys.*, *35*, 5–22, 1994.

Borovikov, L. I., Map of the geological formations of eastern Kazakhstan, 5 sheets, Vses. Nauchno Issled. Geol. Inst., St. Petersburg, 1968.

Butler, R. F., *Paleomagnetism: Magnetic Domains to Geological Terranes*, 319 pp., Blackwell Sci., Malden, Mass., 1992.

Campbell, I. H., and R. W. Griffiths, Implications of mantle plume structure for the evolution of flood basalts, *Earth Planet. Sci. Lett.*, *99*, 79–93, 1990.

Chapin, C. E., and G. R. Lowell, Primary and secondary flow structures in ash-flow tuffs in the Gribbles Run paleovalley, central Colorado, *Spec. Pap. Geol. Soc. Am.*, *180*, 137–154, 1979.

Coleman, R. G., Continental growth in northwest China, *Tectonics*, *8*, 621–635, 1989.

Czamanske, G. K., A. B. Gurevitch, V. Fedorenko, and O. Simonov, Demise of the Siberian plume: Paleogeographic and paleotectonic reconstruction from the prevolcanic and volcanic record, north-central Siberia, *Int. Geol. Rev.*, *40*, 95–115, 1998.

Dalrymple, G. B., G. K. Czamanske, V. A. Fedorenko, O. N. Simonov, M. A. Lanphere, and A. P. Likhachev, A reconnaissance $^{40}Ar/^{39}Ar$ geochronologic study of ore-bearing and related rocks, Siberian Russia, *Geochim. Cosmochim. Acta*, *59*, 2071–2083, 1995.

Didenko, A. N., A. A. Mossakovsky, D. M. Pechersky, S. V. Ruzhentsev, S. G. Samygin, and T. N. Kheraskova, Geodynamics of the central-Asian Paleozoic oceans, *Russ. Geol. Geophys.*, *35*, 48–61, 1994.

Dobretsov, N. L., Permian-Triassic magmatism and sedimentation in Eurasia as a result of a superplume, *Dokl. Akad. Nauk, Engl. Transl.*, *354*, 497–500, 1997.

Dunlop, D. J., and O. Ozdemir, *Rock Magnetism: Fundamentals and Frontiers*, 573 pp., Cambridge Univ. Press, New York, 1997.

Ebinger, C. J., and N. H. Sleep, Cenozoic magmatism throughout east Africa resulting from impact of a single plume, *Nature*, *395*, 788–791, 1998.

Elkins-Tanton, L. T., and B. H. Hager, Melt intrusion as a trigger for lithospheric foundering and the eruption of the Siberian flood basalts, *Geophys. Res. Lett.*, *27*, 3937–3940, 2000.

Enkin, R. J., Z. Yang, Y. Chen, and V. Courtillot, Paleomagnetic constraints on the geodynamic history of the major blocks of China from the Permian to the present, *J. Geophys. Res.*, *97*, 13,953–13,989, 1992.

Ermolov, P. V., and A. E. Izokh, The petrology of the magmatic rocks of the Semeitau volcanic series, *Sov. Geol. Geophys.*, *18*, 52–62, 1977.

Fisher, R. A., Dispersion on a sphere, *Proc. R. Soc. London, Ser. A*, *217*, 295–305, 1953.

Geismann, J. W., R. Van der Voo, and K. L. Howard, A paleomagnetic study of the structural deformation in the Yerrington district, Nevada, *Am. J. Sci.*, *282*, 1042–1109, 1982.

Grommé, C. S., E. H. McKee, and M. C. Blake, Paleomagnetic correlations and potassium–argon dating of middle Tertiary ash-flow sheets in the eastern Great Basin, Nevada and Utah, *Geol. Soc. Am. Bull.*, *83*, 1619–1638, 1972.

Hagstrum, J. T., and P. B. Gans, Paleomagnetism of the Oligocene Kalamazoo tuff: Implications for middle Tertiary extension in east central Nevada, *J. Geophys. Res.*, *94*, 1827–1842, 1989.

Hagstrum, J. T., and P. W. Lipman, Paleomagnetism of the structurally deformed Latir volcanic field, northern New Mexico: Relations to formation of the Questa caldera and development of the Rio Grande Rift, *J. Geophys. Res.*, *91*, 7383–7402, 1986.

Hawkesworth, C. J., K. Gallagher, S. Kelley, M. Mantovani, D. W. Peate, M. Regelous, and N. W. Rogers, Paraná magmatism and the opening of the South Atlantic, in *Magmatism and the Causes of Continental Breakup*, edited by B. C. Storey, T. Alabaster, and R. J. Pankhurst, Geol. Soc. Spec. Publ., 68, 221–240, 1992.

Istomin, A. N., and I. Z. Salmeneva, New data on the Triassic age of the Semeitau volcanic complex (in Russian), *Izv. Acad. Nauk Kazakhstan SSR, Ser. Geol.*, *9*, 86–89, 1964.

Izokh, A., Semeytauskaya vulkano-plutonicheskaya bazit-granitoidnaya seriya, in *Orogennyy Magmatizm Ofiolitovykh Poyasov*, edited by P. V. Ermolov, pp. 144–177, Tr. Inst. Geol. I Geofiz., Novosibirsk, Russia, 1983.

Jaeger, J. C., Cooling and solidification of igneous rocks, in *Basalts: The Poldervaart Treatise on Rocks of Basaltic Composition*, edited by H. H. Hess and A. Poldervaart, pp. 503–536, John Wiley, New York, 1968.

Kamo, S. L., G. K. Czamanske, and T. E. Krogh, A minimum U–Pb age for Siberian flood-basalt volcanism, *Geochim. Cosmochim. Acta*, *60*, 3505–3512, 1996.

Khramov, A. N., *Paleomagnetology*, 308 pp., Springer-Verlag, New York, 1982.

King, S. D., and D. L. Anderson, Edge-driven convection, *Earth Planet. Sci. Lett.*, *160*, 289–296, 1998.

Kirschvink, J., The least-squares line and plane and the analysis of paleomagnetic data, *Geophys. J. R. Astron. Soc.*, *62*, 699–718, 1980.

Kostitsyn, Y. A., K–Ar Dates for the Kazakhstan granites: An overview, in *Granite Related Ore Deposits of Central Kazakhstan and Adjacent Areas*, edited by V. V. Shatov, pp. 387–399, Glagol, St. Petersburg, 1996.

Krestnikov, V. N., and G. I. Reysner, Neotectonic of eastern Kazakhstan and Dzungaria, *Geotectonics*, *1*, 106–113, 1967.

Kumpan, A. S., B. S. Rusinov, and L. E. Sholpo, Results of paleomagnetic studies in central Kazakhstan, *Akad. Nauk SSSR Izv. Earth Phys. Ser.*, 96–103, 1986. (Available in IAGA paleomagnetic database, compiled by M. W. McElhinny and J. Lock, electronic access available at http://www.ngu.no/dragon/Palmag/paleomag.htm.)

Kurchavov, A. M., and V. V. Yarmolyuk, Distribution of Permian continental volcanics in central Asia and tectonic interpretation, *Geotectonics*, *18*, 344–353, 1985.

Larson, R. L., Latest pulse of Earth: Evidence for a mid-Cretaceous superplume, *Geology*, *19*, 547–550, 1991.

Lipman, P. W., The roots of ash flow calderas in western North America: Windows into the tops of granitic batholiths, *J. Geophys. Res.*, *89*, 8801–8841, 1984.

McFadden, P. L., and M. W. McElhinny, The combined analysis of remagnetization circles and direct observations in paleomagnetism, *Earth Planet. Sci. Lett.*, *87*, 161–172, 1988.

McIntosh, W. C., Evaluation of paleomagnetism as a correlation criteria for Mogollon-Datil ignimbrites, southwestern New Mexico, *J. Geophys. Res.*, *96*, 13,459–13,483, 1991.

Merrill, R. T., M. W. McElhinny, and P. T. McFadden, *The Magnetic Field of the Earth: Paleomagnetism, the Core, and the Deep Mantle*, 531 pp., Academic, San Diego, Calif., 1996.

Min, K., R. Mundil, P. R. Renne, and K. R. Ludwig, A test for systematic errors in $^{40}Ar/^{39}Ar$ geochronology through comparison with U-Pb analysis of a 1.1 Ga rhyolite, *Geochim. Cosmochim. Acta*, *64*, 73–98, 2000.

Mohr, P., and B. Zanettin, The Ethiopian flood basalt province, in *Continental Flood Basalts*, edited by J. D. Macdougall, pp. 63–110, Kluwer Acad., Norwell, Mass., 1988.

Palmer, H. C., W. D. MacDonald, C. S. Gromme, and B. B. Ellwood, Magnetic properties and emplacement of the Bishop tuff, California, *Bull. Volcanol.*, *58*, 101–116, 1996.

Prévot, M., A. E. Manikinen, S. Grommé, and A. Lecaille, High paleointensities of the geomagnetic field from thermomagnetic studies on rift valley pillow basalts from the Mid-Atlantic Ridge, *J. Geophys. Res.*, *88*, 2316–2326, 1983.

Pullaiah, G. E., E. Irving, K. L. Buchan, and D. J. Dunlop, Magnetization changes caused by burial and uplift, *Earth Planet. Sci. Lett.*, *28*, 133–143, 1975.

Renne, P. R., and A. R. Basu, Rapid eruption of the Siberian Traps flood basalts at the Permo-Triassic boundary, *Science*, *253*, 176–179, 1991.

Renne, P. R., Z. Zhang, M. A. Richards, M. T. Black, and A. R. Basu, Synchrony and causal relations between Permo-Triassic boundary crises and Siberian Flood Volcanism, *Science*, *246*, 1413–1416, 1995.

Renne, P. R., K. Deckart, M. Ernesto, G. Féraud, and E. M. Piccirillo, Age of the Ponta Grossa dike swarm (Brazil) and implications for Paraná flood volcanic province, *Earth Planet. Sci. Lett.*, *144*, 199–212, 1996.

Renne, P. R., W. D. Sharp, A. L. Deino, G. Orsi, and L. Civetta, $^{40}Ar/^{39}Ar$ dating into the historical realm: Calibration against Pliny the Younger, *Science*, *277*, 1279–1280, 1997.

Renne, P. R., C. C. Swisher, A. L. Deino, D. B. Karner, T. Owens, and D. J. DePaolo, Intercalibration of Standards, Absolute Ages and Uncertainties in $^{40}Ar/^{39}Ar$ Dating, *Chem. Geol.*, *145*, 117–152, 1998.

Rusinov, B. S., Eastern Kazakhstan volcanics, paleomagnetic directions and pole positions, Data for the USSR Issue 6, Sov. Geophys. Comm., World Data Cent.-B, Moscow, 1986. (Available in IAGA paleomagnetic database, compiled by M. W. McElhinny and J. Lock, electronic access available at http://www.ngu.no/dragon/Palmag/paleomag.htm.).

Şengör, A. M. C., and B. A. Natal'in, Paleotectonics of Asia: Fragments of a synthesis, in *The Tectonic Evolution of Asia*, edited by A. Yin and M. Harrison, pp. 486–640, Cambridge Univ. Press, New York, 1996.

Sholpo, L. E., and B. S. Rusinov, Kiiminsk group, Paleomagnetic directions and pole positions, Data for the USSR Issue 1, Sov. Geophys. Comm., World Data Cent.-B, Moscow, 1971. (Available in IAGA paleomagnetic database, compiled by M. W. McElhinny and J. Lock, electronic access available at http://www.ngu.no/dragon/Palmag/paleomag.htm.).

Smethurst, M. A., A. N. Khramov, and T. H. Torsvik, The Neoproterozoic and Palaeozoic palaeomagnetic data for the Siberian platform: From Rodinia to Pangaea, *Earth Sci. Rev.*, *43*, 1–24, 1998.

Van der Voo, R., *Paleomagnetism of the Atlantic, Tethys and Iapetus Oceans*, 411 pp., Cambridge Univ. Press, New York, 1993.

Venkatesan, T. R., A. Kumar, K. Gopalan, and A. I. Al'Mukham, $^{40}Ar/^{39}Ar$ age of Siberian basaltic volcanism, *Chem. Geol.*, *138*, 303–310, 1997.

Watson, G. S., Analysis of dispersion on a sphere, *Mon. Not. R. Astron. Soc.*, *7*, 153–159, 1956.

White, R., and D. McKenzie, Magmatism at rift zones: The generation of volcanic continental margins and flood basalts, *J. Geophys. Res.*, *94*, 7685–7729, 1989.

Zhao, X., R. S. Coe, Y. Zhou, H. Wu, and J. Wang, New paleomagnetic results from northern China: Collision and suturing with Siberia and Kazakhstan, *Tectonophysics*, *181*, 43–81, 1990.

R. S. Coe, J. J. Lyons, and X. Zhao, Earth Sciences Department, University of California, Santa Cruz, CA 95064, USA. (rcoe@es.ucsc.edu; jlyons@es.ucsc.edu; xzhao@es.ucsc.edu)

A. E. Izokh, A. Y. Kazansky, L. V. Kungurtsev, and D. V. Mitrokhin, United Institute of Geology, Geophysics, and Mineralogy Siberian Branch, Russian Academy of Sciences, Akademik Koptug ave. 3, Novosibirsk, 630090 Russia. (kaz@uiggm.nsc.ru)

P. R. Renne, Berkeley Geochronology Center, 2455 Ridge Rd., Berkeley, CA 94709, USA. (prenne@bgc.org)